Geochemical Perspectives Letters

Cerium isotopic constraints on oceanic redox conditions: Insights from first-principles calculations

H.-C. Duan[1,2*], Z.-C. Xiao[1,2], F. Huang[1,2]

https://doi.org/10.7185/geochemlet.2609

Abstract

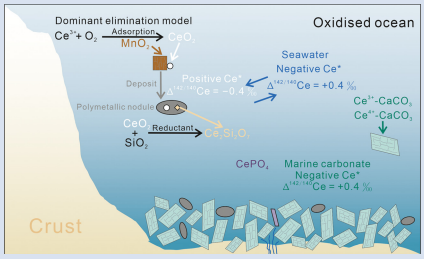

Oceanic redox conditions are important for understanding life explosions, mass extinctions and surface environments. Stable cerium (Ce) isotopes may provide a useful proxy for oceanic redox conditions by combining Ce anomalies in stratigraphic profiles. However, the quantitative response of Ce isotope compositions to redox conditions has yet to be investigated. Here, we estimate equilibrium Ce isotope fractionation factors between marine authigenic minerals to constrain Ce isotope compositional variations under different redox conditions using first-principles calculations. Cerium isotope fractionations ($10^3\ln\alpha_{Total}$) between minerals are controlled by mass-dependent ($10^3\ln\alpha_{Mass}$) and mass-independent isotope fractionation factors ($10^3\ln\alpha_{NVE}$). Our results show that the magnitude of $10^3\ln\alpha_{NVE}$ is comparable to or even larger than that of $10^3\ln\alpha_{Mass}$. The $10^3\ln^{142/140}\alpha_{Total}$ values between seawater and minerals are +0.40, −0.34, +0.11 and −0.07 ‰ for manganese oxides, phosphates and Ce^{3+}- and Ce^{4+}-doped calcites, respectively. In a locally oxidised ocean, the precipitation of manganese oxides increases the Ce isotope composition ($\delta^{142/140}$Ce) of seawater; in an anaerobic ocean, the precipitation of phosphates decreases the $\delta^{142/140}$Ce value of seawater. Therefore, calcite can faithfully record seawater $\delta^{142/140}$Ce values because of the limited Ce isotope fractionations in those redox conditions.

Received 28 April 2025 | Accepted 2 March 2026 | Published 2 April 2026

Introduction

Oceanic redox conditions critically impacted palaeoclimate, palaeoenvironment and life evolution throughout the Earth's history (Bellefroid *et al.*, 2018). Cerium (Ce) has been used as a sensitive proxy for redox conditions because Ce^{4+} distinguishes itself from other trivalent rare earth elements (REEs) during precipitation processes in oxidised oceans, shifting Ce concentrations relative to those of neighbouring elements (known as the Ce anomaly; Tostevin, 2021; Zhang and Shields, 2022). Specifically, trivalent Ce cations in the ocean are oxidised to tetravalent Ce by adsorption onto iron and manganese oxides, and Ce is eliminated from seawater *via* manganese oxide precipitation (Ohta and Kawabe, 2001). This process produces a positive Ce anomaly in the deposited oxides and seawater preserves a negative anomaly (Nozaki and Alibo, 2003). Subsequently, seawater REE features, including negative Ce anomalies, can be recorded in marine calcites because of their comparable partitioning coefficients when incorporated into the calcite lattice (Voigt *et al.*, 2017). This framework is one of the foundations for understanding palaeo-ocean redox conditions from marine carbonates (*e.g.*, Kamber *et al.*, 2004; Tostevin, 2021; Zhang and Shields, 2023).

Negative Ce anomalies in ferromanganese nodules can be ascribed to the input of hydrothermal REEs during diagenetic processes (Elderfield and Greaves, 1981); siderophores and other organic ligands can also produce Ce anomalies *via* bio-mediated Ce oxidation under anaerobic conditions (Kraemer and Bau, 2022). Meanwhile, positive Ce anomalies can be imprinted in marine carbonates by porewaters, masking primary seawater values (Zhang and Shields, 2023). These results indicate that Ce anomalies are not always linked to the oxidation state during oxidative weathering (*e.g.*, Li *et al.*, 2023; Bai *et al.*, 2024) and that a change in oxidation state does not necessarily generate Ce anomalies in ferromanganese oxides (Nakada *et al.*, 2017). Additionally, redox-independent Ce anomalies have been observed in banded iron formations (*e.g.*, Bonnand *et al.*, 2023), complicating the relationship between Ce anomalies and oxidation state. Thus, utilising Ce anomalies to reconstruct the palaeo-oceanic environment requires additional constraints.

Cerium isotopes can be a powerful tool for tracking redox conditions because they are significantly fractionated during oxidative adsorption on ferromanganese oxides (Nakada *et al.*, 2013). Under ambient conditions, Ce isotopes are only slightly fractionated during spontaneous precipitation and ferric oxide adsorption, but significant fractionations occur during manganese oxide adsorption (Nakada *et al.*, 2013, 2017) and ferromanganese oxide formation in hot springs (Nakada *et al.*, 2016). Although Ce isotope compositions in weathering profiles correlate with the average Ce valence state, there is no correlation between the Ce anomaly and average valence state (Li *et al.*, 2023; Bai *et al.*, 2024), indicating that it may be more straightforward to use Ce isotopes to trace redox conditions. However, the mechanism of Ce isotope fractionation in Ce-bearing minerals,

1. State Key Laboratory of Lithospheric and Environmental Coevolution, School of Earth and Space Sciences, University of Science and Technology of China, Hefei 230026, China
2. CAS Center for Excellence in Comparative Planetology, Hefei 230026, China
* Corresponding author (e-mail: duanhc@ustc.edu.cn)

such as calcite, has not been investigated, limiting our understanding of palaeo-ocean environments.

Many stable isotopes undergo mass-dependent fractionations, whereas Ce isotopes also undergo mass-independent fractionations (Schauble, 2023). Mass-independent Ce isotope fractionations mainly result from the nuclear volume effect (NVE) because the anharmonic vibration and Born-Oppenheimer approximation are negligible for heavy elements (Bigeleisen, 1996). First-principles calculations are a powerful tool for estimating mass-dependent equilibrium isotope fractionation factors between complex minerals, fluids and melts (*e.g.*, Rabin *et al.*, 2023; Duan and Huang, 2024). All-electron molecular Dirac-Hartree-Fock calculations have been used to explore relativistic electron configurations and determine the impact of the NVE on Hg, Tl and Pb isotope fractionations in cluster models (Schauble, 2007). Here, we use a methodology developed for periodic boundary conditions to understand the impact of the NVE on Ce isotope fractionations between minerals (Schauble, 2013).

In this study, we calculated the mass-dependent and mass-independent equilibrium Ce isotope fractionation factors ($10^3\ln\alpha_{Mass}$ and $10^3\ln\alpha_{NVE}$) between marine authigenic minerals

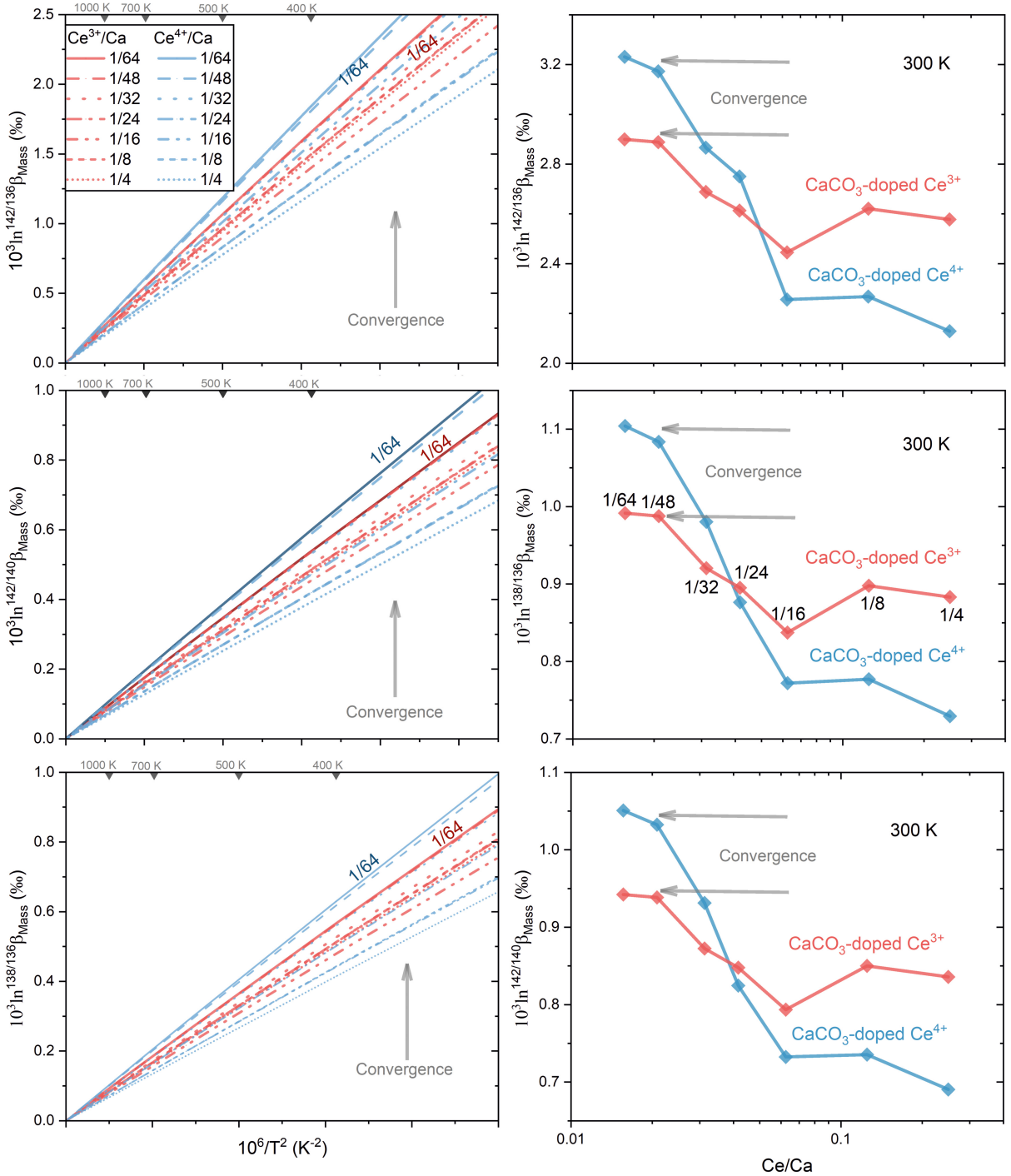

Figure 1 $10^3\ln\beta$ *versus* $10^6/T^2$ (left panels) and Ce/Ca (right panels) in Ce-bearing calcites. In Ce^{3+}-doped calcites and Ce^{4+}-doped calcites, $10^3\ln^{142/136}\beta_{Mass}$, $10^3\ln^{138/136}\beta_{Mass}$, and $10^3\ln^{142/140}\beta_{Mass}$ values increase as Ce/Ca decreases from 1/4 to 1/48, then converge as Ce/Ca further decreases from 1/48 to 1/64.

to construct how Ce isotopes respond to marine redox changes. Cerium removal from oxidised oceans is dominated by the precipitation of manganese oxides. On these surfaces, aqueous Ce species are oxidised to form CeO_2 (Ohta and Kawabe, 2001; Marcus *et al.*, 2018). Cerium removal from anaerobic oceans is controlled by the crystallisation of phosphates, such as monazite and florencite (Manceau *et al.*, 2025). Although calcite is not the primary mineral influencing Ce fluxes, the trace amounts of Ce found in various carbonate rocks can indicate the characteristics of Ce isotopes in seawater. Ce is a trace element in carbonates and may be incorporated into calcite in the same manner as boron (Phillips *et al.*, 2023). We investigated Ce incorporation in calcite using $(Ce^{3+} + Na^{+})$–2 Ca^{2+} and Ce^{4+}–2 Ca^{2+} configurations with Ce/Ca ratios ranging from 1/4 to 1/64 (Fig. S-1). We calculated equilibrium Ce isotope fractionation factors between Ce^{3+}- and Ce^{4+}-doped calcites, cerianite (CeO_2), percleveite ($Ce_2Si_2O_7$), monazite ($CePO_4$) and florencite ($CeAl_3(PO_4)_2(OH)_6$) to explore the impact of redox conditions on Ce isotope compositions in oceans.

Results and Discussion

The effect of Ce concentration on $10^3ln\beta$. The chemical composition can influence reduced partition function ratios ($10^3ln\beta_{Mass}$) by altering the concentration, bond length, coordination number and electronegativity of substituted elements (Méheut *et al.*, 2009). Since Ce is a trace element in calcite, we need to examine concentration and isotope effects of Ce/Ca on $10^3ln\beta_{Mass}$. In Ce^{3+}-doped calcites, $10^3ln^{138/136}\beta$, $10^3ln^{142/140}\beta$ and $10^3ln^{142/136}\beta$ increase as Ce/Ca decreases from 1/4 to 1/48, but they converge to 0.99, 0.94 and 2.90 ‰, respectively, when Ce/Ca decreases from 1/48 to 1/64 (Fig. 1). The discrepancies in calculated $10^3ln^{138/136}\beta$, $10^3ln^{142/140}\beta$ and $10^3ln^{142/136}\beta$ values between Ce/Ca = 1/48 and 1/64 are less than 0.01 ‰, which is significantly lower than the analytical errors on natural samples. Therefore, the effect of Ce concentrations on these $10^3ln\beta_{Mass}$ value in Ce^{3+}-doped calcites is negligible when Ce/Ca < 1/48. The Ce^{4+}-doped calcites exhibit a similar relationship between $10^3ln\beta_{Mass}$ and Ce/Ca, with a limited difference of 0.06 ‰ between Ce/Ca = 1/48 and 1/64. Meanwhile, Ce–O bond lengths also stabilise at certain values as the Ce/Ca decreases to 1/48 and 1/64 in Ce^{3+}- and Ce^{4+}-doped calcites (Table S-1). Hence, the $10^3ln\beta_{Mass}$ values in Ce^{3+}- and Ce^{4+}-doped calcites with Ce/Ca = 1/64 can represent Ce dilution in natural calcites. This concentration and isotope effect implies that for trace elements in minerals, we should calculate isotope fractionation factors in supercells until the fluctuation of $10^3ln\beta_{Mass}$ is smaller than the measurement uncertainty.

Nuclear volume effect on $10^3ln\alpha$. The equilibrium Ce isotope fractionation factors between minerals and florencite are composed of mass-dependent and mass-independent parts ($10^3ln\alpha_{Total} = 10^3ln\alpha_{Mass} + 10^3ln\alpha_{NVE}$). The values of $10^3ln^{138/136}\alpha_{Mass}$, $10^3ln^{142/140}\alpha_{Mass}$ and $10^3ln^{142/136}\alpha_{Mass}$ decrease in the following sequence: Ce^{4+}-doped calcite, Ce^{3+}-doped calcite, percleveite, monazite and cerianite (Fig. S-5a–c). Additionally, $10^3ln^{142/136}\alpha_{Mass}$ is larger than $10^3ln^{138/136}\alpha_{Mass}$ in the same mineral, whereas $10^3ln^{142/140}\alpha_{Mass}$ is similar to $10^3ln^{138/136}\alpha_{Mass}$. This is consistent with the prediction of mass-dependent isotope fractionation theory based on the mass difference between Ce isotopes (Urey, 1947). In contrast, there is no common consensus across the $^{138}Ce/^{136}Ce$, $^{142}Ce/^{140}Ce$ and $^{142}Ce/^{136}Ce$ nuclide ratios for mass-independent equilibrium Ce isotope fractionation factors. For example, at 300 K, $10^3ln^{142/140}\alpha_{NVE}$ and $10^3ln^{142/136}\alpha_{NVE}$ have approximately the same negative values and decrease in the following sequence: monazite, percleveite, cerianite, Ce^{4+}-doped calcite and Ce^{3+}-doped calcite. However, $10^3ln^{138/136}\alpha_{NVE}$ values are limited to the range 0.001 to 0.005 ‰ and decrease in the opposite sequence (Fig. S-5d–f). This result indicates that, unlike those in $^{142}Ce/^{140}Ce$ and $^{142}Ce/^{136}Ce$ pairs, the Ce isotope fractionation factors in the $^{138}Ce/^{136}Ce$ pair are unaffected by the NVE (Fig. 2a). The difference in the mean-squared nuclear radii ($\langle r \rangle^2$) between the ^{138}Ce and ^{136}Ce nuclides is −0.002 $Å^2$, whereas those between

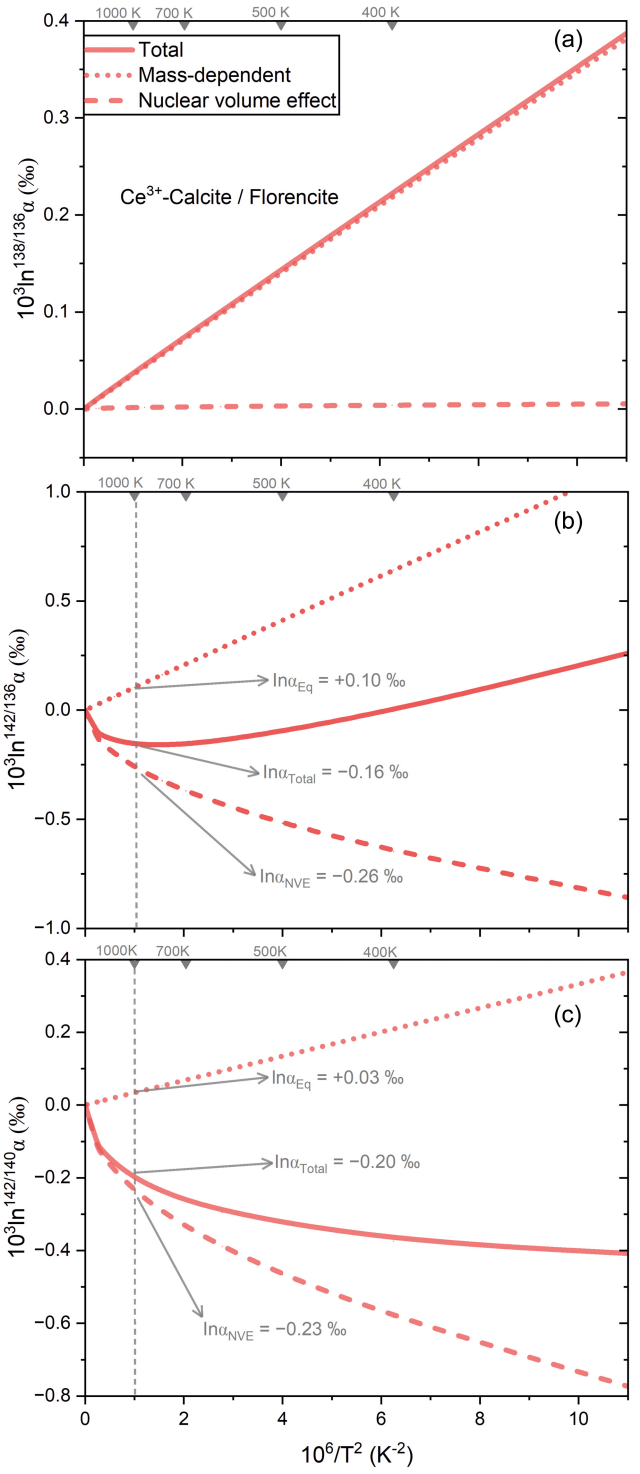

Figure 2 The effect of nuclear volume on Ce isotope fractionations between minerals. Mass-dependent, mass-independent, and total equilibrium Ce isotope fractionation factors of $10^3ln^{142/136}\alpha$, $10^3ln^{138/136}\alpha$ and $10^3ln^{142/140}\alpha$ between Ce^{3+}-calcite and florencite are compared as a case study.

^{142}Ce and ^{140}Ce nuclides and between ^{142}Ce and ^{136}Ce nuclides are +0.281 and +0.312 Å^2, respectively. Because $10^3\ln\alpha_{NVE}$ depends on the electron density around the nucleus and $[r]^2$ (Bigeleisen, 1996; Schauble, 2013), the difference in $[r]^2$ dominates the difference among $10^3\ln^{138/136}\alpha_{NVE}$, $10^3\ln^{142/140}\alpha_{NVE}$ and $10^3\ln^{142/136}\alpha_{NVE}$.

At 300 K, the $10^3\ln^{142/136}\alpha_{Mass}$ and $10^3\ln^{142/136}\alpha_{NVE}$ values of Ce^{3+}-doped calcite are +1.13 and −0.86 ‰, respectively, implying that the absolute value of $10^3\ln^{142/136}\alpha_{Total}$ is smaller than those of $10^3\ln^{142/136}\alpha_{Mass}$ and $10^3\ln^{142/136}\alpha_{NVE}$ because of their opposite isotope fractionation directions. At 300 K, the $10^3\ln^{142/140}\alpha_{Mass}$ and $10^3\ln^{142/140}\alpha_{NVE}$ values of Ce^{3+}-doped calcite are +0.37 and −0.78 ‰, respectively, implying that the NVE is about twice as significant as the mass-dependent fractionation and dominates the Ce isotope fractionation directions. These results indicate that the NVE impact on Ce isotope fractionation factors cannot be neglected, especially under high-temperature conditions (Fig. 2b,c). Overall, the measurable Ce isotope fractionation between Ce-bearing minerals indicates that Ce isotopes recorded in stratigraphic profiles can be used to reconstruct redox conditions of palaeo-oceans.

Implications for palaeo-seawater redox conditions. Cerium fluctuations in seawater are influenced by specific minerals precipitating. The Ce flux in oxidised oceans is predominantly regulated by manganese oxide precipitation because Ce^{3+} can be oxidised and adsorbed onto the surface of manganese oxides to form tetravalent Ce oxides (CeO_2) (Takahashi *et al.*, 2000; Nakada *et al.*, 2013), removing Ce and producing negative Ce anomalies in seawater (Fig. 3). Because REEs do not fractionate significantly during incorporation into calcite (Voigt *et al.*, 2017), calcite precipitates capture the negative Ce anomalies of oxidised oceans. In contrast, phosphate precipitation dominates the Ce flux in anaerobic oceans because Ce cations and $CePO_4$ clusters can be incorporated into phosphatic lattices (Manceau *et al.*, 2025), which does not produce Ce anomalies in calcites. These

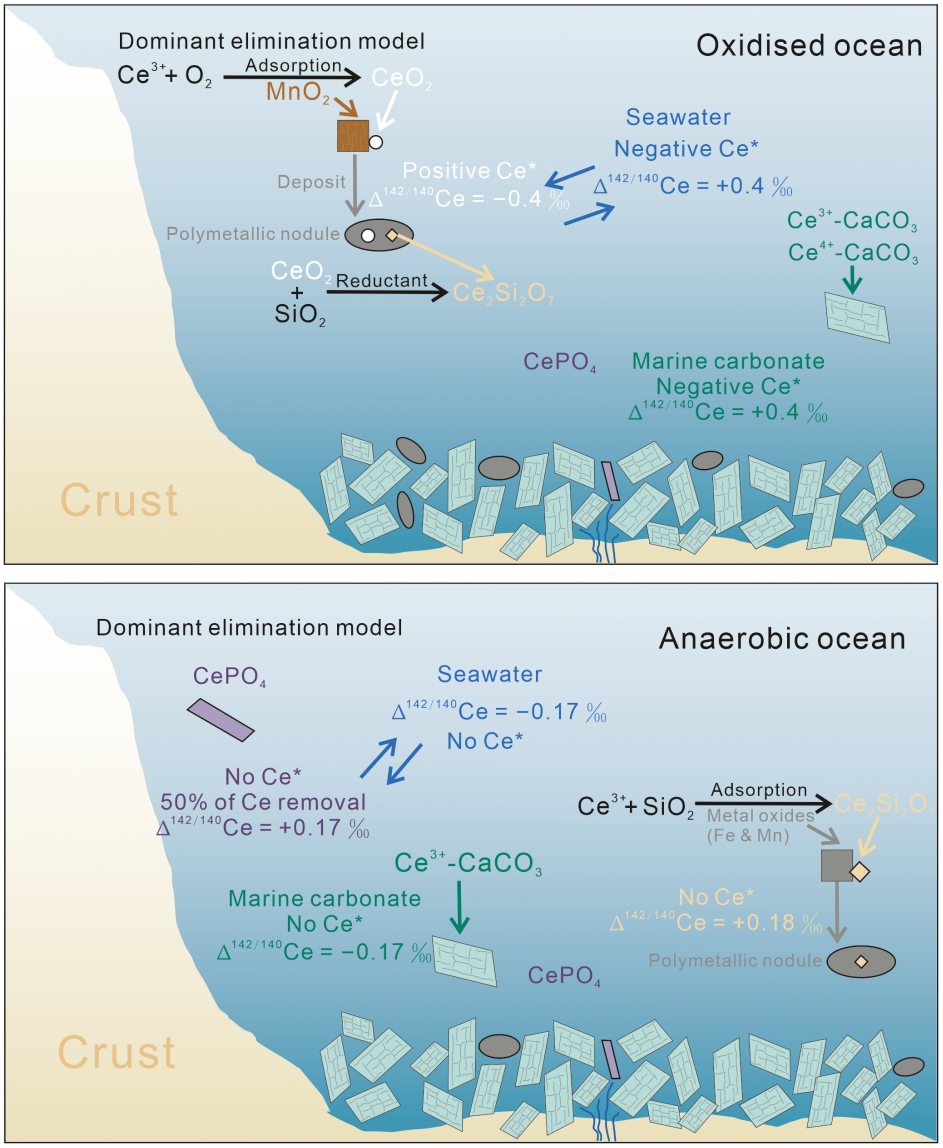

Figure 3 Schematic diagrams of Ce isotope variations in oxidised and anaerobic ocean domains. The initial Ce isotope composition ($\delta^{142/140}$Ce) of seawater is assumed to be 0.0 ‰. We assumed that Ce flux (*ca.* 90 %) is primarily controlled by the precipitation of manganese oxides in oxidised oceans, but is governed by phosphate precipitation (*ca.* 50 %) in anaerobic oceans. Under seawater conditions at pH 8, the Ce isotope fractionation factors between seawater and minerals are shown in Table S-3. Deposition of manganese oxides can increase $\delta^{142/140}$Ce values in seawater, which are otherwise decreased by the deposition of phosphates. Calcite can therefore reflect the $\delta^{142/140}$Ce value of seawater with limited Ce isotope fractionation at pH 8.

processes can lead to significant differences in Ce isotope compositions between seawater, manganese oxides, carbonates and phosphates, which may provide a promising tool for investigating oceanic redox conditions (*e.g.*, Nakada *et al.*, 2013; Bonnand *et al.*, 2023; Li *et al.*, 2023; Bai *et al.*, 2024). However, quantitative Ce isotope fractionation factors have not yet been investigated for these processes. This study shows that the $10^3\ln^{142/140}\alpha_{Total}$ values of manganese oxides (CeO_2), phosphates ($CePO_4$) and Ce^{3+}- and Ce^{4+}-doped calcites are −0.55, +0.04, −0.41, and −0.24 ‰, respectively (Table S-2), providing a theoretical foundation for tracing redox conditions.

To construct oceanic redox models, we developed a series of models to simulate changing $\delta^{142/140}Ce$ values under different redox conditions by Rayleigh and batch isotope fractionations (Wang *et al.*, 2021). Variations of $\delta^{142/140}Ce$ in seawater during mineral precipitation can be described by Rayleigh fractionation as:

$$\delta^{142/140}Ce_{SW} = (\delta^{142/140}Ce_{SW0}+10^3)f^{\alpha_{A-B}-1} - 10^3 \quad \text{(Eq. 1)}$$

Variations of $\delta^{142/140}Ce$ in seawater during mineral precipitation can also be described by batch fractionation as:

$$\delta^{142/140}Ce_{SW} = \delta^{142/140}Ce_{SW0}+(1-f)\times(10^3\ln\alpha_{A-B})10^3 \quad \text{(Eq. 2)}$$

In Equations (1) and (2), $\delta^{142/140}Ce_{SW}$ and $\delta^{142/140}Ce_{SW0}$ represent the Ce isotope compositions in instantaneous and initial seawater, respectively. Phase A and B represent precipitated minerals and seawater, respectively. The $\delta^{142/140}Ce_{SW0}$ value is assumed to be 0.0 ‰. The $10^3\ln^{142/140}\alpha_{Total}$ value of cerianite (CeO_2) can be considered a substitute for that of manganese oxides because CeO_2 is the primary form of Ce absorbed onto manganese oxides. At 300 K, the difference between the $10^3\ln^{142/140}\alpha_{Total}$ values of monazite ($CePO_4$) and florencite ($CeAl_3(PO_4)_2(OH)_6$) is limited to +0.04 ‰ (Table S-2); therefore we use the $10^3\ln^{142/140}\alpha_{Total}$ value of $CePO_4$ to represent that for phosphates. The metal species present in fluids significantly influence isotope fractionations between minerals and fluids (Duan and Huang, 2025). The abundance of aqueous Ce species, including Ce^{3+}, $Ce(OH)^{2+}$, $Ce(CO_3)^+$ and $Ce(CO_3)_2^-$, changes with seawater pH (*e.g.*, Nakada *et al.*, 2013, 2017). Ce^{3+} is the dominant species at a pH of *ca.* 5; under these conditions, the $10^3\ln^{142/140}\alpha_{Total}$ value between seawater and manganese oxides is about +0.4 ‰ (Nakada *et al.*, 2017). Based on the relationship of calculated $10^3\ln^{142/140}\alpha_{Total}$ values between phosphates and manganese oxides, $10^3\ln^{142/140}\alpha_{Total}$ values between seawater and phosphates are about −0.19 ‰ (Fig. 4). These Ce isotope fractionation factors and Ce isotope compositions of seawater throughout geological history can be adjusted appropriately to consider different pH conditions, dominant species and compositional values in future works.

These simulations demonstrate that manganese oxide precipitation increases seawater $\delta^{142/140}Ce$ values, whereas phosphate precipitation reduces seawater $\delta^{142/140}Ce$ values (Fig. 4). If precipitated particles are suspended in the euphotic zone for an extended period of time and reach equilibrium with seawater, the batch fractionation model should control the Ce isotope fractionation between deposited phosphate or manganese particles and seawater. In the batch isotope fractionation model, the respective $\delta^{142/140}Ce$ values of seawater and deposited manganese nodules increase from 0.0 and −0.4 ‰ to +0.4 and 0.0 ‰. Similarly, the respective $\delta^{142/140}Ce$ values of seawater and deposited phosphates decrease from 0.0 ‰ to −0.2 ‰ and +0.2 ‰ to 0.0 ‰. These findings imply that $\Delta^{142/140}Ce$ between seawater and precipitated particles is consistent with their $10^3\ln^{142/140}\alpha_{Total}$ values and is unrelated to the proportion of Ce removal (*f*). In contrast, if precipitated particles are rapidly removed from surface seawater, the change of seawater $\delta^{142/140}Ce$ values should be controlled by Rayleigh fractionation. When *f* is less than 50 %, the $\delta^{142/140}Ce$ values of seawater and deposited minerals in the Rayleigh fractionation model are similar to those in the batch fractionation model. However, when *f* is larger than 50 %, the $\delta^{142/140}Ce$ value of seawater may increase to +1.0 ‰ or decrease to −0.5 ‰ with the precipitation of uniquely manganese oxides or uniquely phosphates, respectively. Hence, it is essential to consider the proportion of Ce removal and $10^3\ln^{142/140}\alpha_{Total}$ during precipitation when assessing $\delta^{142/140}Ce$ variations in seawater.

Finally, we explore another isotope box model based on actual seawater conditions, assuming a pH of 8 and $\delta^{142/140}Ce_{SW0} = 0$ ‰. $Ce(CO_3)^+$ and $Ce(CO_3)_2^-$ are major aqueous Ce species, and the $10^3\ln^{142/140}\alpha_{Total}$ value between seawater

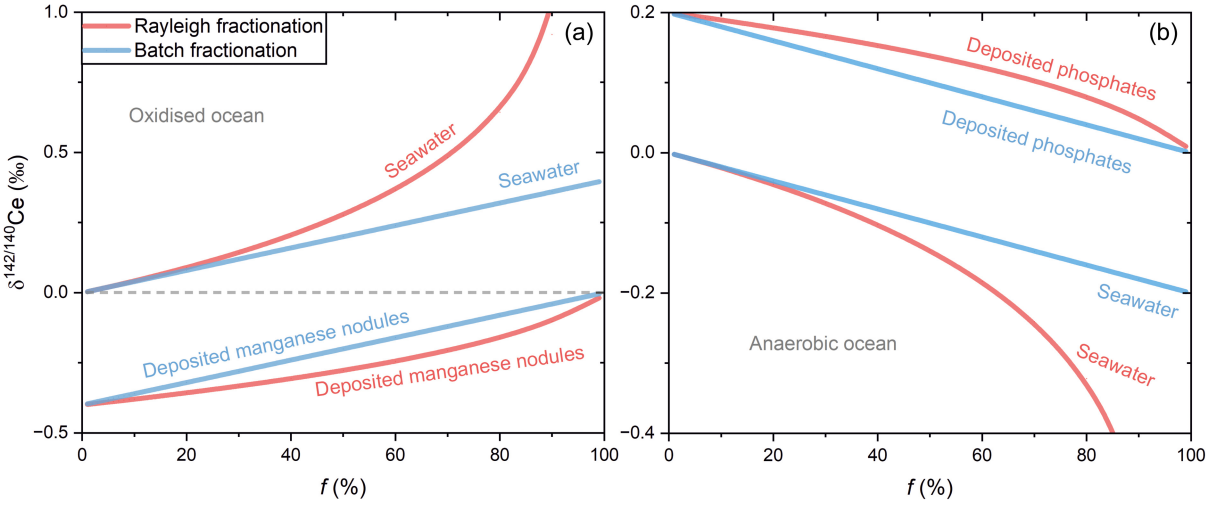

Figure 4 The Ce isotope variation model as Ce is eliminated from **(a)** oxidised and **(b)** anaerobic oceans. The initial Ce isotope composition ($\delta^{142/140}Ce$) of seawater is assumed to be 0.0 ‰. The equilibrium Ce isotope fractionation factors between seawater and manganese oxide, and between seawater and phosphates are set to +0.4 ‰ and −0.19 ‰, respectively, based on this study and prior experimental results (Nakada *et al.*, 2013; Bonnand *et al.*, 2023). The proportion of Ce removal is represented as *f* (%). The Ce isotope fractionation factors between minerals calculated herein were used for Rayleigh and batch isotope fractionation models at 300 K.

and manganese oxides is about +0.25 ‰ in this condition (Nakada *et al.*, 2017). Based on our calculated $10^3\ln^{142/140}\alpha_{Total}$ values in Ce-bearing minerals, the $10^3\ln^{142/140}\alpha_{Total}$ value between seawater and phosphates is about −0.34 ‰; the $10^3\ln^{142/140}\alpha_{Total}$ values between seawater and Ce^{3+}-doped calcites and between seawater and Ce^{4+}-doped calcites are about +0.11 and −0.07 ‰, respectively (Table S-3). Whereas the distribution of Ce oxidation states in calcites remains unknown, the Ce isotope fractionation between seawater and calcites with a dominant tetravalent or trivalent form has been constrained. In well-oxygenated oceans (as at present), manganese oxides precipitate out of the ocean, removing almost all soluble Ce by CeO_2 adsorption ($f > 90$ %; Nozaki and Alibo, 2003; Nakada *et al.*, 2017). Based on batch fractionation models, the deposited manganese oxides have $\delta^{142/140}Ce \approx 0.0$ ‰, similar to initial seawater compositions. The $\delta^{142/140}Ce$ value of seawater should increase to + 0.4 ‰, and deposited calcites can record such high $\delta^{142/140}Ce$ signatures and negative Ce anomalies because of limited Ce isotope fractionation between seawater and calcite (Fig. 3). In anaerobic oceans, Ce removal is dominated by phosphate precipitation. If we assume that 50 % of the Ce is removed from seawater through phosphate precipitation, then the deposited phosphates and seawater exhibit $\delta^{142/140}Ce$ values of +0.17 and −0.17 ‰, respectively. Hence, deposited calcites in anaerobic oceans can record low $\delta^{142/140}Ce$ signatures of −0.17 ‰ without any Ce anomaly. These findings show that the $\delta^{142/140}Ce$ values of deposited calcites, phosphates, and manganese oxides are significantly different in oxidised or anaerobic oceans, implying that a shift of $\delta^{142/140}Ce$ values in stratigraphic profiles may be utilised to signal the redox conditions of the ocean. The pH and Ce species in seawater should be considered in different conditions, as they will affect assessments of the Ce isotope fractionation factors between minerals and seawater. Importantly, mineralogical analyses of sedimentary rocks, particularly the ratios of carbonate to phosphate and manganese oxide, are the foundation for the application of Ce isotopes to infer marine redox conditions.

Acknowledgements

The Supercomputing Center at the University of Science and Technology of China and Hefei Advanced Computing Center provided resources to enable computations. This work is supported by the National Natural Science Foundation of China (grants 42494854, 42303030 and 42330101) and the International Postdoctoral Exchange Fellowship (YJ20220411) of the Office of China Postdoc Council. We appreciate editorial handling by Claudine Stirling and thank our anonymous reviewers for their constructive suggestions.

Editor: Claudine Stirling

Additional Information

Supplementary Information accompanies this letter at https://www.geochemicalperspectivesletters.org/article2609.

Cite this letter as: Duan, H.-C., Xiao, Z.-C., Huang, F. (2026) Cerium isotopic constraints on oceanic redox conditions: Insights from first-principles calculations. *Geochem. Persp. Let.* 39, 29–35. https://doi.org/10.7185/geochemlet.2609

References

Bai, J., Wu, C., Wu, H., Wang, Z., Zhang, L., Zhong, S., Ma, J., Wei, G. (2024) $\delta^{142}Ce$ minus $\delta^{146}Nd$ value as a redox indicator in Earth's surface environments. *Earth Planetary Science Letters* 629, 118597. https://doi.org/10.1016/j.epsl.2024.118597

Bellefroid, E.J., Hood, A.v.S., Hoffman, P.F., Thomas, M.D., Reinhard, C.T., Planavsky, N.J. (2018) Constraints on Paleoproterozoic atmospheric oxygen levels. *Proceedings of the National Academy of Sciences* 115, 8104–8109. https://doi.org/10.1073/pnas.1806216115

Bigeleisen, J. (1996) Nuclear Size and Shape Effects in Chemical Reactions. Isotope Chemistry of the Heavy Elements. *Journal of the American Chemical Society* 118, 3676–3680. https://doi.org/10.1021/ja954076k

Bonnand, P., Boyet, M., Bosq, C. (2023) Stable cerium isotopes as a tracer of oxidation reactions. *Geochemical Perspectives Letters* 28, 27–30. https://doi.org/10.7185/geochemlet.2340

Duan, H., Huang, F. (2024) Equilibrium indium isotope fractionation between indium-bearing minerals: Insights from first-principles calculations. *Geochimica et Cosmochimica Acta* 369, 51–61. https://doi.org/10.1016/j.gca.2024.01.031

Duan, H., Huang, F. (2025) Equilibrium indium isotope fractionation in chloride-rich aqueous solutions using first-principles calculations. *Geochimica et Cosmochimica Acta* 393, 304–317. https://doi.org/10.1016/j.gca.2025.01.026

Elderfield, H., Greaves, M.J. (1981) Negative cerium anomalies in the rare earth element patterns of oceanic ferromanganese nodules. *Earth and Planetary Science Letters* 55, 163–170. https://doi.org/10.1016/0012-821X(81)90095-9

Kamber, B.S., Bolhar, R., Webb, G.E. (2004) Geochemistry of late Archaean stromatolites from Zimbabwe: evidence for microbial life in restricted epicontinental seas. *Precambrian Research* 132, 379–399. https://doi.org/10.1016/j.precamres.2004.03.006

Kraemer, D., Bau, M. (2022) Siderophores and the formation of cerium anomalies in anoxic environments. *Geochemical Perspectives Letters* 22, 50–55. https://doi.org/10.7185/geochemlet.2227

Li, W., Liu, X.-M., Nakada, R., Takahashi, Y., Hu, Y., Shakouri, M., Zhang, Z., Okumura, T., Yamada, S. (2023) The cerium isotope fingerprints of redox fluctuation in bauxites. *Earth and Planetary Science Letters* 602, 117962. https://doi.org/10.1016/j.epsl.2022.117962

Marcus, M., Toner, B., Takahashi, Y. (2018) Forms and distribution of Ce in a ferromanganese nodule. *Marine Chemistry* 202, 58–66. https://doi.org/10.1016/j.marchem.2018.03.005

Manceau, A., Gaillot, A., Liao, J., Li, Y., Mathon, O., Lomachenko, K., Glatzel, P., Simionovici, A., Balvay, M., Paul, S., Koschinsky, A., Steinmann, S. (2025) Cerium occurs as cerium-phosphate clusters around bioapatite nanocrystals in deep-sea sediments. *Communications Earth and Environment* 6, 466. https://doi.org/10.1038/s43247-025-02439-2

Méheut, M., Lazzeri, M., Balan, E., Mauri, F. (2009) Structural control over equilibrium silicon and oxygen isotopic fractionation: A first-principles density-functional theory study. *Chemical Geology* 258, 28–37. https://doi.org/10.1016/j.chemgeo.2008.06.051

Nakada, R., Takahashi, Y., Tanimizu, M. (2013) Isotopic and speciation study on cerium during its solid–water distribution with implication for Ce stable isotope as a paleo-redox proxy. *Geochimica et Cosmochimica Acta* 103, 49–62. https://doi.org/10.1016/j.gca.2012.10.045

Nakada, R., Takahashi, Y., Tanimizu, M. (2016) Cerium stable isotope ratios in ferromanganese deposits and their potential as a paleo-redox proxy. *Geochimica et Cosmochimica Acta* 181, 89–100. https://doi.org/10.1016/j.gca.2016.02.025

Nakada, R., Tanaka, M., Tanimizu, M., Takahashi, Y. (2017) Aqueous speciation is likely to control the stable isotopic fractionation of cerium at varying pH. *Geochimica et Cosmochimica Acta* 218, 273–290. https://doi.org/10.1016/j.gca.2017.09.019

Nozaki, Y., Alibo, D.S. (2003) Importance of vertical geochemical processes in controlling the oceanic profiles of dissolved rare earth elements in the northeastern Indian Ocean. *Earth and Planetary Science Letters* 205, 155–172. https://doi.org/10.1016/S0012-821X(02)01027-0

Ohta, A., Kawabe, I. (2001) REE(III) adsorption onto Mn dioxide (δ-MnO_2) and Fe oxyhydroxide: Ce(III) oxidation by δ-MnO_2. *Geochimica et Cosmochimica Acta* 65, 695–703. https://doi.org/10.1016/S0016-7037(00)00578-0

Phillips, B., Chen, Z., Rasbury, E. (2023) Boron coprecipitation with calcite: distinguishing calcite-hosted B by NMR spectroscopy. *ACS Earth and Space Chemistry* 7, 2430–2443. https://doi.org/10.1021/acsearthspacechem.3c00198

Rabin, S., Blanchard, M., Pinilla, C., Poitrasson, F., Grégoire, M. (2023) Iron and silicon isotope fractionation in silicate melts using first-principles molecular dynamics. *Geochimica et Cosmochimica Acta* 343, 212–233. https://doi.org/10.1016/j.gca.2022.11.017

Schauble, E.A. (2007) Role of nuclear volume in driving equilibrium stable isotope fractionation of mercury, thallium, and other very heavy elements. *Geochimica et Cosmochimica Acta* 71, 2170–2189. https://doi.org/10.1016/j.gca.2007.02.004

Schauble, E.A. (2013) Modeling nuclear volume isotope effects in crystals. *Proceedings of the National Academy of Sciences* 110, 17714–17719. https://doi.org/10.1073/pnas.1216216110

Schauble, E.A. (2023) Nuclear volume isotope fractionation of europium and other lanthanide elements. *Geochemical Journal* 57, 118–133. https://doi.org/10.2343/geochemj.GJ23010

Takahashi, Y., Shimizu, H., Usui, A., Kagi, H., Nomura, M. (2000) Direct observation of tetravalent cerium in ferromanganese nodules and crusts by X-ray-absorption near-edge structure (XANES). *Geochimica et Cosmochimica Acta* 64, 2929–2935. https://doi.org/10.1016/S0016-7037(00)00403-8

Tostevin, R. (2021) Cerium Anomalies and Paleoredox. *Cambridge University Press*. https://doi.org/10.1017/9781108847223

Urey, H.C. (1947) The thermodynamic properties of isotopic substances. *Journal of the Chemical Society (Resumed)*, 562–581. https://doi.org/10.1039/jr9470000562

Voigt, M., Mavromatis, V., Oelkers, E.H. (2017) The experimental determination of REE partition coefficients in the water-calcite system. *Chemical Geology* 462, 30–43. https://doi.org/10.1016/j.chemgeo.2017.04.024

Wang, W., Li, C.-H., Brodholt, J.P., Huang, S., Walter, M.J., Li, M., Wu, Z., Huang, F., Wang, S.-J. (2021) Sulfur isotopic signature of Earth established by planetesimal volatile evaporation. *Nature Geosciences* 14, 806–811. https://doi.org/10.1038/s41561-021-00838-6

Zhang, K., Shields, G.A. (2022) Sedimentary Ce anomalies: Secular change and implications for paleoenvironmental evolution. *Earth-Science Reviews* 229, 104015. https://doi.org/10.1016/j.earscirev.2022.104015

Zhang, K., Shields, G.A. (2023) Early diagenetic mobilization of rare earth elements and implications for the Ce anomaly as a redox proxy. *Chemical Geology* 635, 121619. https://doi.org/10.1016/j.chemgeo.2023.121619